

1 **Can We Improve the Preprocessing of**  
2 **Photospheric Vector Magnetograms by the**  
3 **Inclusion of Chromospheric Observations?**

4 **T. Wiegelmann**<sup>1</sup> · **J.K. Thalmann**<sup>1</sup> ·  
5 **C.J. Schrijver**<sup>2</sup> · **M.L. DeRosa**<sup>2</sup> · **T.R. Metcalf**<sup>3</sup>  
6 †

7 DOI: 10.1007/s11207-008-9130-y  
8 Bibliographic Code: 2008SoPh..247..249W

9 © Springer ●●●●

10 **Abstract** The solar magnetic field is key to understanding the physical processes  
11 in the solar atmosphere. Nonlinear force-free codes have been shown to be useful  
12 in extrapolating the coronal field upward from underlying vector boundary data.  
13 However, we can only measure the magnetic field vector routinely with high accu-  
14 racy in the photosphere, and unfortunately these data do not fulfill the force-free  
15 condition. We must therefore apply some transformations to these data before non-  
16 linear force-free extrapolation codes can be self-consistently applied. To this end, we  
17 have developed a minimization procedure that yields a more chromosphere-like field,  
18 using the measured photospheric field vectors as input. The procedure includes force-  
19 free consistency integrals, spatial smoothing, and — newly included in the version  
20 presented here — an improved match to the field direction as inferred from fibrils  
21 as can be observed in, *e.g.*, chromospheric H $\alpha$  images. We test the procedure using  
22 a model active-region field that included buoyancy forces at the photospheric level.  
23 The proposed preprocessing method allows us to approximate the chromospheric  
24 vector field to within a few degrees and the free energy in the coronal field to within  
25 one percent.

26 **Keywords:** Magnetic fields, Photosphere, Chromosphere, Corona

27 **1. Introduction**

28 The solar interior, photosphere and atmosphere are coupled by magnetic fields. It  
29 is therefore important to gain insights about the magnetic field structure in all  
30 layers of the Sun and solar atmosphere. Direct and accurate measurements of the  
31 magnetic field vector are typically carried out only on the photosphere. Although  
32 measurements in higher layers are available for a few individual cases, *e.g.* in the  
33 chromosphere by Solanki *et al.* (2003) and in the corona by Lin, Kuhn, and Coul-  
34 ter (2004), the line-of-sight integrated character of such chromospheric and coronal  
35 magnetic field measurements complicates their interpretation (Kramar, Inhester, and  
36 Solanki, 2006). Knowledge of the magnetic field in the corona is essential, however, to

---

†Unfortunately our colleague, co-author, and friend Tom Metcalf deceased before the final manuscript was finished. We continued our joint work in his memory and would like to remember him here.

<sup>1</sup> Max-Planck-Institut für Sonnensystemforschung,  
Max-Planck-Strasse 2, 37191 Katlenburg-Lindau, Germany  
email: wiegelmann@mps.mpg.de email: thalmann@mps.mpg.de

<sup>2</sup> Lockheed Martin Advanced Technology Center, Dept.  
ADBS, Bldg. 252, 3251 Hanover St., Palo Alto, CA 94304,  
USA email: schryver@lmsal.com email: derosa@lmsal.com

<sup>3</sup> Northwest Research Associates, Colorado Research  
Associates Division, 3380 Mitchell Ln., Boulder, CO 90301  
USA

37 understand basic physical processes such as the onset of flares, coronal mass ejections  
 38 and eruptive prominences.

39 Inferences of the coronal magnetic field can be obtained by extrapolating mea-  
 40 surements of the photospheric magnetic field vector (*e.g.* observed by *Hinode*/SOT,  
 41 SOLIS or the upcoming SDO/HMI instruments) into the corona. Because the mag-  
 42 netic pressure dominates the plasma pressure in active-region coronae, making the  
 43 plasma  $\beta$  low, [See work by Gary (2001) and Schrijver and van Ballegooijen (2005),  
 44 which discuss the plasma beta over active regions and over the quiet Sun, respec-  
 45 tively], these extrapolations neglect non-magnetic forces and assume the coronal  
 46 magnetic field  $\mathbf{B}$  to be force-free, such that it obeys:

$$\nabla \cdot \mathbf{B} = 0, \quad (1)$$

$$(\nabla \times \mathbf{B}) \times \mathbf{B} = 0. \quad (2)$$

47 Equation (2) implies that the electric current density  $\mu_0 \mathbf{j} = \nabla \times \mathbf{B}$  is parallel  
 48 to the magnetic field  $\mathbf{B}$ . Starting more than a quarter century ago (Sakurai, 1981),  
 49 different mathematical methods and numerical implementations have been developed  
 50 to solve the nonlinear force-free equations (1) and (2) for the solar case. See, for  
 51 example, (Sakurai, 1989; Amari *et al.*, 1997; Wiegelmann, 2008) for review papers  
 52 and (Schrijver *et al.*, 2006; Metcalf *et al.*, 2007) for evaluations of the performance of  
 53 corresponding computer programs with model data. The codes use the magnetic field  
 54 vector (or quantities derived from the magnetic field vector) on the bottom boundary  
 55 of a computational domain as input. One would like to prescribe the measured  
 56 photospheric data as the bottom boundary of nonlinear force-free fields (NLFFF)  
 57 codes, but there is a problem: the observed photospheric magnetic field is usually not  
 58 force-free. The relatively high plasma  $\beta$  in the photosphere means that non-magnetic  
 59 forces cannot be neglected there and that such photospheric magnetic field data are  
 60 not consistent with well known force-free compatibility conditions defined in (Aly,  
 61 1989). Recently, Wiegelmann, Inhester, and Sakurai (2006) developed a scheme that  
 62 mitigates this problem, in which the inconsistent and noisy photospheric vector mag-  
 63 netograms used as bottom boundary conditions are preprocessed in order to remove  
 64 net magnetic forces and torques and to smooth out small-scale noise-like magnetic  
 65 structures. The resulting magnetic field data are sufficiently force-free and smooth  
 66 for use with extrapolation codes, but also are found to bear a high resemblance to  
 67 chromospheric vector magnetic field data. This leads us to the question whether we  
 68 can constrain the preprocessing tool further by taking direct chromospheric obser-  
 69 vations, such as H $\alpha$  images, into consideration. We will investigate this topic in the  
 70 present work.

## 71 2. A Short Review About Consistency Criteria for Force-free Coronal 72 Extrapolations

73 In this section, we briefly discuss the criteria on the photospheric boundary data that  
 74 are required for consistency with a force-free extrapolation of the overlying coronal  
 75 magnetic field. Molodensky (1969), Molodensky (1974), Aly (1989), and Sakurai  
 76 (1989) show how moments of the Lorentz force, integrated over a volume of interest,  
 77 define constraints on the closed surface bounding this volume. As explained in detail

78 in Molodensky (1974) the sense of these relations is that on average a force-free  
79 field cannot exert pressure on the boundary or shear stresses along axes lying in  
80 the boundary. For the coronal magnetic field extrapolation calculations discussed  
81 here, a localized region of interest, such as an active region, is typically selected  
82 for analysis. The extrapolation algorithms applied to the coronal volume overlying  
83 such localized regions of interest require boundary conditions, and, except at the  
84 lower (photospheric) boundary, these boundary conditions are usually chosen to be  
85 consistent with potential fields and thus do not possess magnetic forces or torques.  
86 In these cases, the consistency criteria reduce to conditions on the lower boundary  
87 only:

88 1. On average force-free fields cannot exert pressure on the boundary

$$F_1 = \int_S B_x B_z dx dy = 0, \quad (3)$$

$$F_2 = \int_S B_y B_z dx dy = 0 \quad (4)$$

$$F_3 = \int_S (B_x^2 + B_y^2) dx dy - \int_S B_z^2 dx dy = 0. \quad (5)$$

89 2. On average force-free fields cannot create shear stresses along axes lying in the  
90 boundary

$$T_1 = \int_S x (B_x^2 + B_y^2) dx dy - \int_S x B_z^2 dx dy = 0, \quad (6)$$

$$T_2 = \int_S y (B_x^2 + B_y^2) dx dy - \int_S y B_z^2 dx dy = 0, \quad (7)$$

$$T_3 = \int_S y B_x B_z dx dy - \int_S x B_y B_z dx dy = 0. \quad (8)$$

91 These relations must be fulfilled in order to be suitable boundary conditions for a  
92 nonlinear force-free coronal magnetic field extrapolation. We define dimensionless  
93 numbers,

$$\epsilon_{\text{force}} = \frac{|F_1| + |F_2| + |F_3|}{\int_S (B_x^2 + B_y^2 + B_z^2) dx dy}, \quad (9)$$

$$\epsilon_{\text{torque}} = \frac{|T_1| + |T_2| + |T_3|}{\int_S \sqrt{x^2 + y^2} (B_x^2 + B_y^2 + B_z^2) dx dy}. \quad (10)$$

94 in order to evaluate how well these criteria are met. Ideally, it is necessary for  $\epsilon_{\text{force}} =$   
95  $\epsilon_{\text{torque}} = 0$  for a force-free coronal magnetic field to exist.

96 Aly (1989) pointed out that the magnetic field is probably not force-free in the  
97 photosphere, where  $\mathbf{B}$  is measured because the plasma  $\beta$  in the photosphere is of  
98 the order of unity and pressure gradient and gravity forces are not negligible. The  
99 integral relations (3)-(8) are not satisfied in this case in the photosphere and the

100 measured photospheric field is not a suitable boundary condition for a force-free  
 101 extrapolation. Investigations by Metcalf *et al.* (1995) revealed that the solar magnetic  
 102 field is not force-free in the photosphere, but becomes force-free about 400km above  
 103 the photosphere. The problem has been addressed also by Gary (2001) who pointed  
 104 out that care has to be taken when extrapolating the coronal magnetic field as a  
 105 force-free field from photospheric measurements, because the force-free low corona  
 106 is sandwiched between two regions (photosphere and higher corona) with a plasma  
 107  $\beta \approx 1$ , where the force-free assumption might break down. An additional problem is  
 108 that measurements of the photospheric magnetic vector field contain inconsistencies  
 109 and noise. In particular the components of  $\mathbf{B}$  transverse to the line of sight, as  
 110 measured by current vector magnetographs, are more uncertain than the line-of-  
 111 sight component. As measurements in higher layers of the solar atmosphere (where  
 112 the magnetic field is force-free) are not routinely available, we have to deal with  
 113 the problem of inconsistent (with the force-free assumption as defined by Equations  
 114 (3)–(8)) photospheric measurements. A routine which uses measured photospheric  
 115 vector magnetograms to find suitable boundary conditions for a nonlinear force-free  
 116 coronal magnetic field extrapolation, dubbed “preprocessing”, has been developed  
 117 by Wiegelmann, Inhester, and Sakurai (2006).

### 118 3. Preprocessing

#### 119 3.1. Classical Preprocessing

120 The preprocessing scheme of Wiegelmann, Inhester, and Sakurai (2006) involves  
 121 minimizing a two-dimensional functional of quadratic form similar to the following:

$$L_{\text{prep}} = \mu_1 L_1 + \mu_2 L_2 + \mu_3 L_3 + \mu_4 L_4 + \mu_5 L_5, \quad (11)$$

122 where

$$L_1 = \left[ \left( \sum_p B_x B_z \right)^2 + \left( \sum_p B_y B_z \right)^2 + \left( \sum_p B_z^2 - B_x^2 - B_y^2 \right)^2 \right], \quad (12)$$

$$L_2 = \left[ \left( \sum_p x (B_z^2 - B_x^2 - B_y^2) \right)^2 + \left( \sum_p y (B_z^2 - B_x^2 - B_y^2) \right)^2 \right. \\ \left. + \left( \sum_p y B_x B_z - x B_y B_z \right)^2 \right], \quad (13)$$

$$L_3 = \left[ \sum_p (B_x - B_{x\text{obs}})^2 + \sum_p (B_y - B_{y\text{obs}})^2 \right. \\ \left. + \sum_p (B_z - B_{z\text{obs}})^2 \right], \quad (14)$$

$$L_4 = \left[ \sum_p (\Delta B_x)^2 + (\Delta B_y)^2 + (\Delta B_z)^2 \right]. \quad (15)$$

123 The surface integrals as defined in Equations (3)–(8) are here replaced by a  
 124 summation  $\sum_p$  over all grid nodes  $p$  of the bottom surface grid. We normalize the  
 125 magnetic field strength with the average magnetic field on the photosphere and the  
 126 length scale with the size of the magnetogram. Each constraint  $L_n$  is weighted by a  
 127 yet undetermined factor  $\mu_n$ . The first term ( $n=1$ ) corresponds to the force-balance  
 128 conditions (3)–(5), the next ( $n=2$ ) to the torque-free condition (6)–(8). The following  
 129 term ( $n=3$ ) contains the difference of the optimized boundary condition with the  
 130 measured photospheric data and the next term ( $n=4$ ) controls the smoothing. The  
 131 2D-Laplace operator is designated by  $\Delta$  and the differentiation in the smoothing  
 132 term is achieved by the usual 5-point stencil. The last term ( $n = 5$ ) has not been  
 133 used in preprocessing so far and will be introduced in the next section. The aim of the  
 134 preprocessing procedure is to minimize  $L_{\text{prep}}$  so that all terms  $L_n$  if possible are made  
 135 small simultaneously. This minimization procedure provides us iterative equations  
 136 for  $B_x, B_y, B_z$  (see Wiegmann, Inhester, and Sakurai (2006) for details). As result  
 137 of the preprocessing we get a data set which is consistent with the assumption of a  
 138 force-free magnetic field in the corona but also as close as possible to the measured  
 139 data within the noise level.

140 Nonlinear force-free extrapolation codes can be applied only to low plasma  $\beta$  re-  
 141 gions, where the force-free assumption is justified. This is known not to be the case in  
 142 the photosphere, but is mostly true for the upper chromosphere and for the corona in  
 143 quiescent conditions. The preprocessing scheme as used until now modifies observed  
 144 photospheric vector magnetograms with the aim of approximating the magnetic field  
 145 vector at the bottom of the force-free domain, *i.e.*, at a height that we assume  
 146 to be located in the middle to upper chromosphere. In this study, we investigate  
 147 whether the use of chromospheric fibril observations as an additional constraint in  
 148 the preprocessing can bring the resulting field into even better agreement with the  
 149 expected chromospheric vector field.

150 We discuss this idea in the next section.

### 151 3.2. H $\alpha$ -Preprocessing

152 The idea is to specify another term ( $\mu_5 L_5$ ) in Equation (11) which measures how  
 153 well the preprocessed magnetic field is aligned with fibrils seen in H $\alpha$ . As a first  
 154 step we have to extract the directions of the fibrils, say  $H_x$  and  $H_y$  out of the H $\alpha$   
 155 images, where  $\mathbf{H}$  is a unit vector tangent ( $|\mathbf{H}| = 1$ ) to the chromospheric fibrils  
 156 projected onto the solar photosphere (representing the field direction with a 180-  
 157 degree ambiguity). For simplicity one might rebin  $H_x$  and  $H_y$  to the same resolution  
 158 as the vector magnetogram. In regions where we cannot identify clear filamentary  
 159 structures in the images we set  $H_x = H_y = 0$ . These regions are only affected by the  
 160 other, classical terms of the preprocessing functional (11). The angle of the projected  
 161 magnetic field vector on the xy-plane with the H $\alpha$  image is

$$\sin(\phi) = \frac{|\mathbf{B}_{\parallel} \times \mathbf{H}|}{|\mathbf{B}_{\parallel}| |\mathbf{H}|} \quad (16)$$

162 where  $\mathbf{B}_{\parallel} = (B_x, B_y)$  is the projection of the magnetic field vector in the xy-plane  
 163 and  $\mathbf{H} = (H_x, H_y)$  are the directions of the chromospheric H $\alpha$  fibrils. The prepro-  
 164 cessing aims for deriving the magnetic field vector on the bottom boundary of the  
 165 force-free domain, which is located in the chromosphere. The chromospheric magnetic  
 166 field is certainly a priori unknown and as initial condition for the preprocessing  
 167 routine we take  $\mathbf{B}_{\parallel}$  from the photospheric vector magnetogram.

168 We define the functional:

$$L_5 = \sum_p w(B_x H_y - B_y H_x)^2 = \sum_p w \mathbf{B}_{\parallel}^2 \sin^2(\phi). \quad (17)$$

169 Please note that the term  $B_x H_y - B_y H_x$  in Equation (17) weights the angle  
 170 with the magnetic field strength, because it is in particular important to minimize  
 171 the angle in strong field regions. The space dependent function  $w = w(x, y)$  is not a  
 172 priori related to the magnetic field strength.  $w$  can be specified in order to indicate the  
 173 confidence level of the fibril direction-finding algorithm (see *e.g.*, Inhester, Feng, and  
 174 Wiegelmann (2007) for the description of a corresponding feature recognition tool).  
 175 For the application to observational data  $w$  will be (with appropriate normalization)  
 176 provided by this tool. It is likely, however, that the direction of the H $\alpha$  fibrils can be  
 177 identified more accurately in strong magnetic field regions, but this is not an a priori  
 178 assumption. In Section 4.3 we investigate the influence of different assumptions for  
 179  $w$ .

180 We take the functional derivative of  $L_5$

$$\frac{dL_5}{dt} = 2(B_x H_y - B_y H_x) \left( H_y \frac{dB_x}{dt} - H_x \frac{dB_y}{dt} \right). \quad (18)$$

181 For a sufficiently small time step  $dt$  we get a decreasing  $L_5$  with the iteration  
 182 equations

$$\frac{dB_x}{dt} = -2w \mu_5 (B_x H_y - B_y H_x) H_y, \quad (19)$$

$$\frac{dB_y}{dt} = 2w \mu_5 (B_x H_y - B_y H_x) H_x. \quad (20)$$

183 The aim of our procedure is to make all terms in functional (11) small simulta-  
 184 neously. There are obvious contradictions between some of the  $L_n$  terms, such as  
 185 between the  $n = 3$  (photospheric data) and  $n = 4$  (smoothing) terms. An important  
 186 task is to find suitable values for the five parameters  $\mu_n$  which control the relative  
 187 weighting of the terms in Equation (11). The absolute values do not matter; only the  
 188 relative weightings are important. We typically give all integral relations of the force  
 189 and torque conditions (3)-(8) the same weighting (unity). To fulfill these consistency  
 190 integrals is essential in order to find suitable boundary conditions for a nonlinear  
 191 force-free extrapolation. In principle it would be possible to examine different values  
 192 for the force-free term  $\mu_1$  and torque-free term  $\mu_2$  -or even to give six different  
 193 weightings for the six integral relations- but giving all integrals the same weighting  
 194 seems to be a reasonable choice. The torque integrals depend on the choice of the  
 195 length scale  $D$  and giving the same weighting to all integrals requires  $\mu_2 = \frac{\mu_1}{D^2}$ . For  
 196 the length scale normalization used here ( $D = 1$ ) this leads to  $\mu_1 = \mu_2$ .

197 We will test our newly developed method with the help of a model active region  
198 in the next section.

## 199 4. Tests

### 200 4.1. An Active Region Model for Testing the New Method

201 We test our extended preprocessing routine with the help of an active region model  
202 recently developed by van Ballegoijen *et al.* (2007) In this model line-of-sight pho-  
203 tospheric measurements from SOHO/MDI have been used to compute a potential  
204 field. A twisted flux rope was then inserted into the volume, after which the whole  
205 system was relaxed towards a nonlinear force-free state with the magnetofrictional  
206 method described in van Ballegoijen (2004). The van Ballegoijen *et al.* (2007)  
207 model is force-free throughout the entire computational domain, except within two  
208 gridpoints of the bottom boundary. Hereafter, we refer to the bottom of the force-free  
209 layer as the “model chromosphere” (see the top panel of Figure 1). On the bottom  
210 boundary (see the central panel of Figure 1), hereafter referred to as the “model  
211 photosphere”, the model contains significant non-magnetic forces and the force-free  
212 consistency criteria (3)-(8) are not satisfied. These forces take the form of vertical  
213 buoyancy forces directed upward, and have been introduced by van Ballegoijen *et al.*  
214 *et al.* (2007) to mimic the effect of a reduced gas pressure in photospheric flux tubes.  
215 The nature of these forces is therefore expected to be similar to those observed on the  
216 real Sun. For a more detailed discussion we refer to Metcalf *et al.* (2007). Both the  
217 chromospheric ( $\mathbf{B}_{\text{ch}}$ ) as well as the photospheric magnetic field vector ( $\mathbf{B}_{\text{ph}}$ ) from  
218 the van Ballegoijen *et al.* (2007) model have been used to test four sophisticated  
219 nonlinear force-free extrapolation codes in a blind algorithm test by Metcalf *et al.*  
220 (2007).<sup>1</sup> The codes computed nonlinear force-free codes in a  $320 \times 320 \times 256$  box,  
221 which is about at the upper limit current codes can handle on workstations. We  
222 briefly summarize the results of Metcalf *et al.* (2007) as:

- 223 • NLFFF-extrapolations from model-chromospheric data recover the original ref-  
224 erence field with high accuracy.
- 225 • When the extrapolations are applied to the model-photospheric data, the ref-  
226 erence field is not well recovered.
- 227 • Preprocessing of the model-photospheric data to remove net forces and torques  
228 improves the result, but the resulting accuracy was lower than for extrapolations  
229 from the model-chromospheric data.

230 The poor performance of extrapolations using the unprocessed model-photospheric  
231 data is related to their inconsistency with respect to the force-free conditions (3)-  
232 (8). The central panel of Figure 1 shows the photospheric magnetic field and the  
233 central panel of Figure 2 illustrates the difference between the model-chromospheric  
234 and model-photospheric fields. It is evident that there are remarkable differences  
235 in all components of the magnetic field vector. For real data we usually cannot  
236 measure the chromospheric magnetic field vector directly (which was possible for

---

<sup>1</sup>Previously, the NLFFF codes have been intensively tested and evaluated with the (Low and Lou, 1990) semi-analytic equilibria (Schrijver *et al.*, 2006).

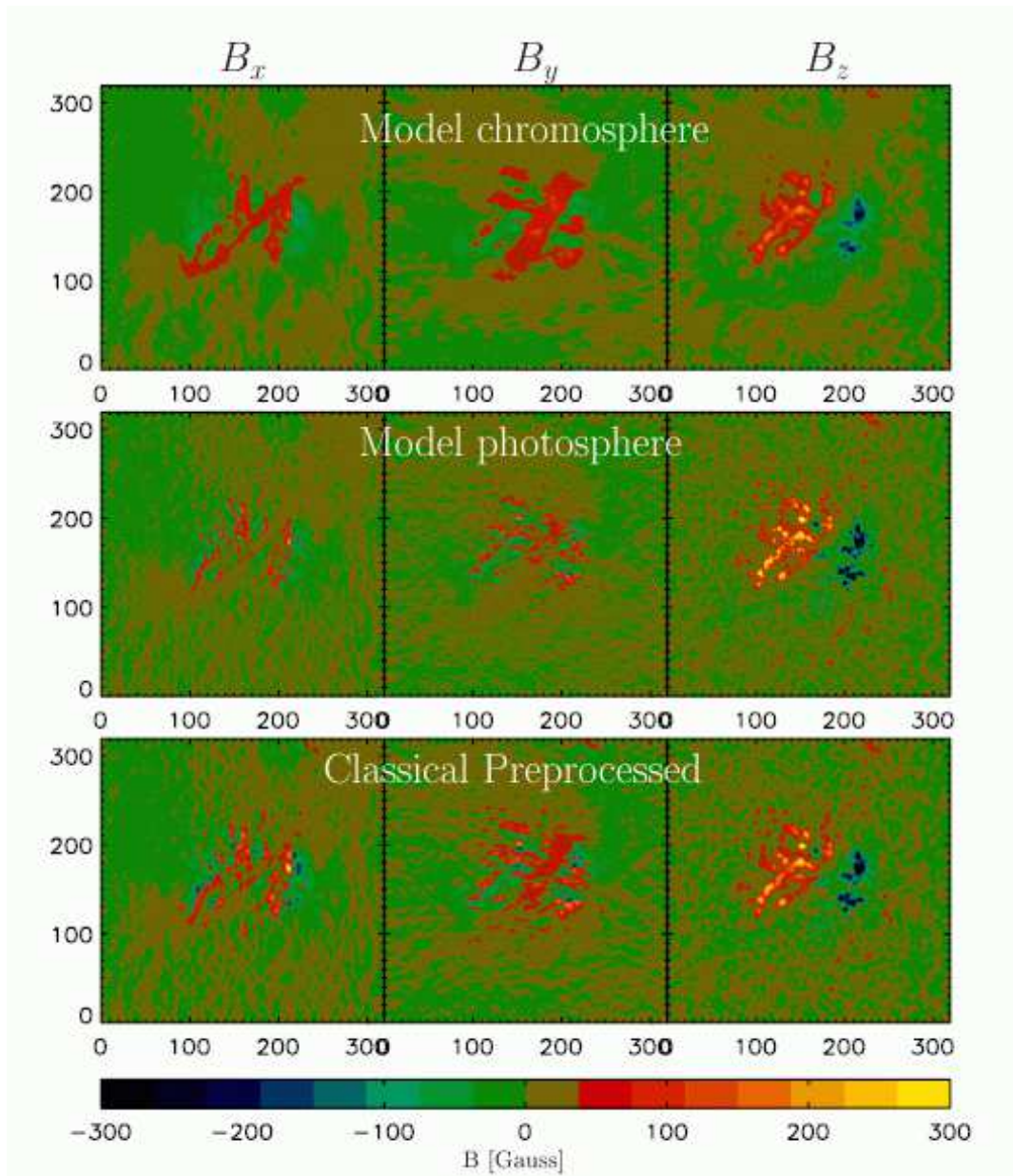


**Figure 1.** Top: Model-chromospheric magnetic field located in the  $z = 2$  layer, Center: Model-photospheric magnetic field, Bottom: Model-photospheric magnetic field after classical preprocessing with  $\mu_3 = 0.025$ ,  $\mu_4 = 0.155$ .



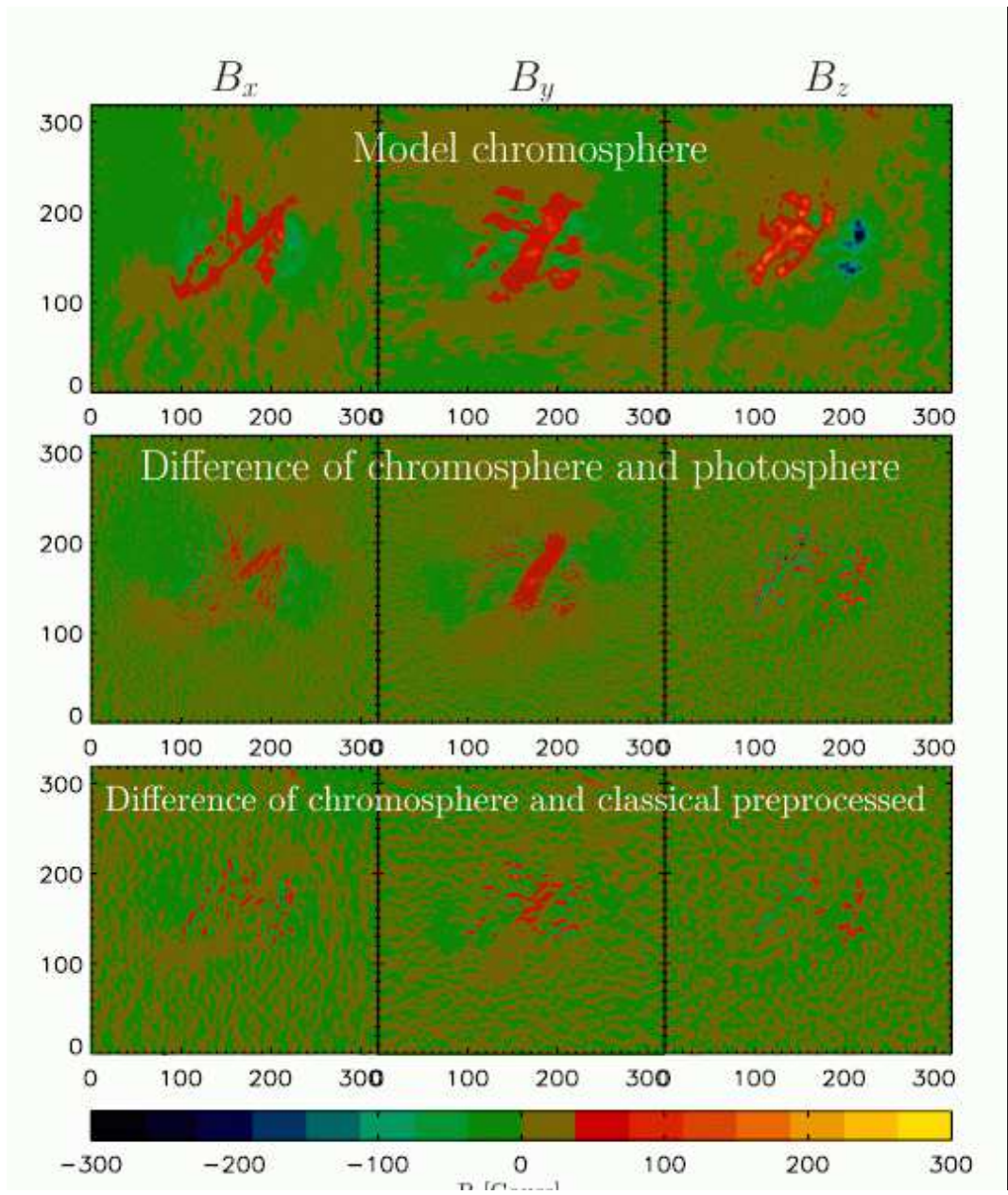


**Figure 2.** Top: Model-chromospheric magnetic field, Center: Difference between the chromospheric and photospheric model vector field, Bottom: Difference between the chromospheric and classical preprocessed photospheric field.

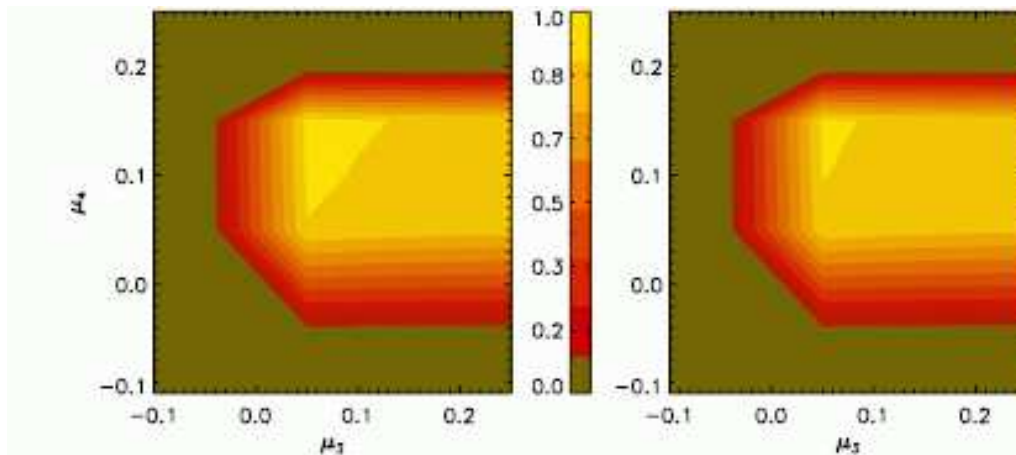


**Figure 3.** Correlation of the preprocessed field (left panel:  $B_x$ , right panel:  $B_y$ ) with the model chromosphere in dependence of the preprocessing parameters  $\mu_3$  and  $\mu_4$ . We found a maximum correlation at  $\mu_3 = 0.025$  and  $\mu_4 = 0.155$ .

237 (van Ballegoijen *et al.*, 2007) model data) and we have to apply preprocessing before  
 238 using the data as input for force-free extrapolation codes. Force-free extrapolations  
 239 using preprocessed data from the model photosphere (as lower panels of Figures 1 and  
 240 2), while encouraging, were not completely satisfactory, in light of the results being  
 241 worse than when the model-chromospheric data were used as boundary conditions. In  
 242 what follows, we will use an artificial  $H\alpha$  image created from the model chromosphere  
 243 to test a modified preprocessing scheme, and compare the results to the classical  
 244 (original) preprocessing scheme.

245 We use the model-chromospheric magnetic field ( $\mathbf{B}_{\text{ch}}$ ) to derive the direction  
 246 vectors of the artificial  $H\alpha$  images. For the model case we can simply use the  
 247 chromospheric model field to specify the direction vectors  $H_x$  and  $H_y$ , which con-  
 248 tain only information regarding the direction of the horizontal components of the  
 249 magnetic field (including a  $180^\circ$  ambiguity, but no information about the magnetic  
 250 field strength. For real data this information can be derived from high-resolution  $H\alpha$   
 251 images using feature recognition techniques, *e.g.* the ridge detector of Inhester, Feng,  
 252 and Wiegelmann (2007).

#### 253 4.2. Optimal Parameter Set for Classical Preprocessing

254 We tested more than 1000 possible combinations of  $\mu_3$  and  $\mu_4$  using the model-  
 255 photospheric field as input, and computed the Pearson correlation coefficient between  
 256 the preprocessed results and the model-chromospheric field. Only  $B_x$  and  $B_y$  were  
 257 used in computing the correlation coefficient, because the correlation of the longitudi-  
 258 nal (*i.e.*, the line-of-sight) component is in general higher than that of the transverse  
 259 components, due to  $B_z$  not being affected by the ambiguity-problem and the noise  
 260 being much lower than in the other directions.

261 We computed 100 combinations of  $\mu_3$  and  $\mu_4$  between  $-0.2 \leq \mu_3, \mu_4 \leq 0.2$   
 262 with a step size of  $\Delta\mu_3 = \Delta\mu_4 = 0.05$ . Hereafter a local maximum around  $\mu_3 =$   
 263  $0.05$  and  $\mu_4 = 0.15$  appeared. This region was analyzed in more detail by using these

264 two values as new initial guess. To do this, we tried another 100 combinations around  
 265 this pair with a reduced step size of  $\Delta\mu_3 = \Delta\mu_4 = 0.005$  in the positive as well as  
 266 the negative direction. Then the absolute maximum of the correlation coefficients for  
 267 both,  $B_x$  and  $B_y$  appeared at  $\mu_3 = 0.025$  and  $\mu_4 = 0.155$  (see Figure 3). The bottom  
 268 panel of Figure 1 shows the corresponding preprocessed photospheric magnetic field.

#### 269 4.3. Optimal Parameters and Weighting Functions for H $\alpha$ Preprocessing.

270 In the following we aim to find suitable parameters for including information from  
 271 H $\alpha$  images into the preprocessing.

272 Our main aim is to investigate the effects of additional chromospheric informa-  
 273 tion. To exclude side effects we therefore keep the combination of  $\mu_1$ - $\mu_4$  found in  
 274 the previous section to be able to clearly investigate the effect of the additional  
 275 term  $L_5$ . In principle one could vary all  $\mu_n$  simultaneously. We cannot exclude that  
 276 there might exist a better combination of  $\mu_1$  to  $\mu_5$  with better agreement of our  
 277 preprocessed field and the model chromospheric field. This is, however, not the aim  
 278 of this work, because this is not a suitable way to deal with real data, because there  
 279 is no model chromosphere to test the result. It is not possible to provide an optimal  
 280 parameter set suitable for all vector magnetographs. The optimal combination has  
 281 to be carried out for different instruments separately. We expect that an optimal  
 282 parameter set for a certain instrument and particular region will be also useful for  
 283 the preprocessing of other regions of the same kind (say active regions) observed  
 284 with the same instrument.

285 We test our methods with “model fibrils” extracted from the model chromosphere  
 286 shown in the top panel of Figure 4. We define  $w(x, y)$  used in Equation (17) as one  
 287 of the following:

- 288 1. We assume that at every point of our H $\alpha$  image gives us the exact orientation  
 289 of the magnetic field (which is indeed the case, as we calculated it from the  
 290 chromospheric model data) and fix our weighting with  $w(x, y) = w_1 = 1$ .
- 291 2. We assume that the photospheric magnetic field magnitude gives us the impor-  
 292 tance of the H $\alpha$  information at each point and use

$$294 \quad w(x, y) = w_2 = \sqrt{(B_x^2 + B_y^2 + B_z^2)_{\text{ph}}}.$$

295 We scale  $w_2$  to a maximum value of 1. (See Figure 4 bottom left panel.)

- 296 3. We do as in the previous case, but assume now, that only points in the magne-  
 297 togram where the field magnitude is greater than 50 % of the maximum contribute  
 298 to the H $\alpha$  preprocessing. So, we define

$$299 \quad w(x, y) = w_3 = \begin{cases} 1 & \text{for } w_2 \geq 0.5 \\ 0 & \text{for } w_2 < 0.5 \end{cases}.$$

300 (See Figure 4 bottom center panel.)

- 301 4. In our last case we assume in the same way as in the previous one, but now only  
 302 points in the magnetogram where the field magnitude is greater than 10 % of the  
 303 maximum contribute to the preprocessing. All these grid points are weighted with  
 304 1 and the rest with zero. In other words, one defines

$$305 \quad w(x, y) = w_4 = \begin{cases} 1 & \text{for } w_2 \geq 0.1 \\ 0 & \text{for } w_2 < 0.1 \end{cases}.$$

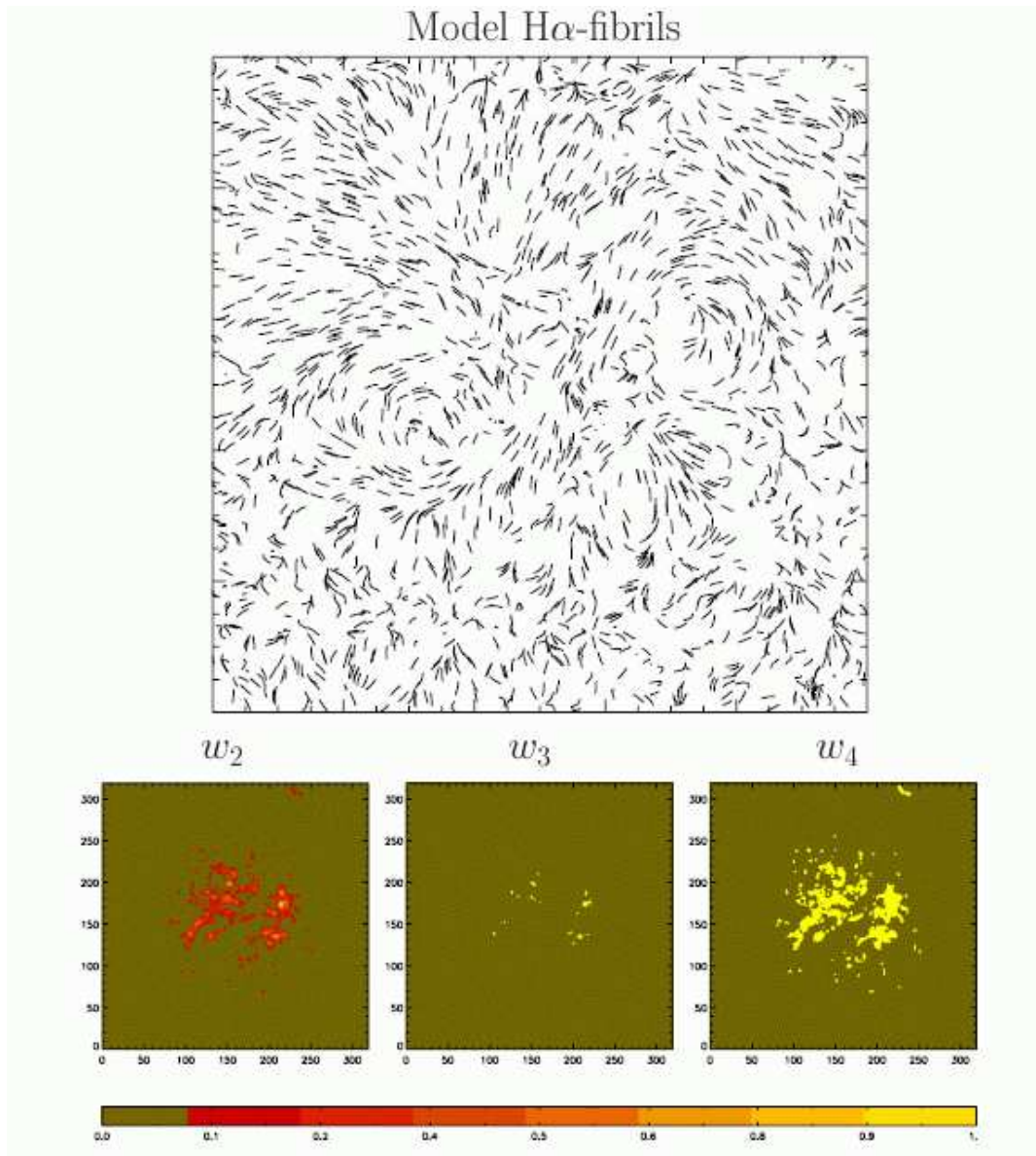


**Figure 4.** Top: H $\alpha$  fibrils identified from the model chromosphere. The fibrils give us information about the transverse components ( $B_x$  and  $B_y$ ) of the chromospheric magnetic field. The fibrils contain a  $180^\circ$  ambiguity and do not provide any information about the chromospheric magnetic field strength. The bottom panels show from left to right the different weighting functions  $w_2$ ,  $w_3$ ,  $w_4$ , respectively. Regions where  $w$  is higher are more important in the  $L_5$ -preprocessing-term (17) which controls the influence of the H $\alpha$ -fibrils.

306 (See Figure 4 bottom right panel.)

307 We now figure out the optimal value of  $\mu_5$  in Equation (11) for the four different  
 308 weighting functions  $w_1 - w_4$ . Initially, we use a step size of  $\Delta\mu_5 = 0.05$  and then,  
 309 around the first appearing maximum, we reduced it to  $\Delta\mu_5 = 0.005$ . This is to  
 310 find a more precise optimal value of  $\mu_5$ . We calculate the Pearson correlation coeffi-  
 311 cient between the chromospheric reference field ( $\mathbf{B}_{\text{ch}}$ ) and the minimum solution of  
 312 the preprocessing routine ( $\mathbf{B}_{\text{pp}}$ ). This provides us the optimal values of  $\mu_5$  for the  
 313 different weighting functions, see second row in Table 1.

## 314 5. Results

315 Table 1 lists some metrics related to the various preprocessing schemes, including the  
 316 dimensionless numbers  $\epsilon_{\text{force}}$  and  $\epsilon_{\text{torque}}$  from Equations (9) and (10), the values  
 317 of the various  $L_n$  from Section 3, and the averaged angles between the prepro-  
 318 cessing results and the model-chromospheric field. The first three rows of the table  
 319 list the model chromosphere ( $B_{\text{ch}}$ ) and photosphere ( $B_{\text{ph}}$ ) data and the classical  
 320 preprocessing scheme ( $B_{\text{cp}}$ ). When using the unprocessed model-photospheric data  
 321 ( $B_{\text{ph}}$ ), it is clear that the force-free consistency criteria (as represented by  $L_{12}$ ,  
 322  $\epsilon_{\text{force}}$ , and  $\epsilon_{\text{torque}}$ ) are not fulfilled and are orders of magnitude higher than for the  
 323 chromospheric data ( $B_{\text{ch}}$ ). Consequently, we cannot expect the extrapolation codes  
 324 to result in a meaningful nonlinear force-free field in the corona, as discussed in  
 325 Metcalf *et al.* (2007).

326 The remaining rows in Tables 1 and 2 list the results for the cases where the H $\alpha$   
 327 preprocessing was used. A qualitative comparison of the H $\alpha$ -preprocessed magne-  
 328 tograms (shown in Figure 5) with the model chromosphere (shown in the top panel  
 329 of Figure 1) indicates a strong resemblance for all three magnetic field components,  
 330 but certainly not a perfect match. Difference images between the H $\alpha$ -preprocessed  
 331 magnetograms and the model chromosphere (shown in the top panel of Figure 1)  
 332 are present in Figure 6. The resemblance using the H $\alpha$  preprocessing scheme is  
 333 much improved when compared to the magnetograms resulting from the classical  
 334 preprocessing scheme.

335 Table 2 displays metrics of the resulting nonlinear force-free extrapolations using  
 336 each preprocessing scheme.<sup>2</sup> As expected, the extrapolation codes perform poorly  
 337 when the unprocessed boundary ( $B_{\text{ph}}$ ) is used. In particular, the resulting magnetic  
 338 energy  $\epsilon_{\text{mag}}$  of this case (normalized to the energy of the reference solution) is only  
 339 65% of the correct answer, making it almost impossible to estimate the free magnetic  
 340 energy in the solution available for release during eruptive processes such as flares  
 341 and coronal mass ejections.

342 Taking preprocessing into account (rows 3-7 in both tables) significantly improves  
 343 the result. The force-free consistency criteria ( $L_{12}$ ,  $\epsilon_{\text{force}}$ ,  $\epsilon_{\text{torque}}$ ) are adequately  
 344 fulfilled for all preprocessed cases and are even better (lower values) than the model  
 345 chromospheric field. This is naturally, however, because the preprocessing routine has  
 346 been developed in particular to derive force-free-consistent boundary conditions from

---

<sup>2</sup>For an explanation of the extrapolation method used to perform the results in Table 2, see appendix A and references therein. An explanation of the vector comparison metrics used in the table is given in Appendix B.

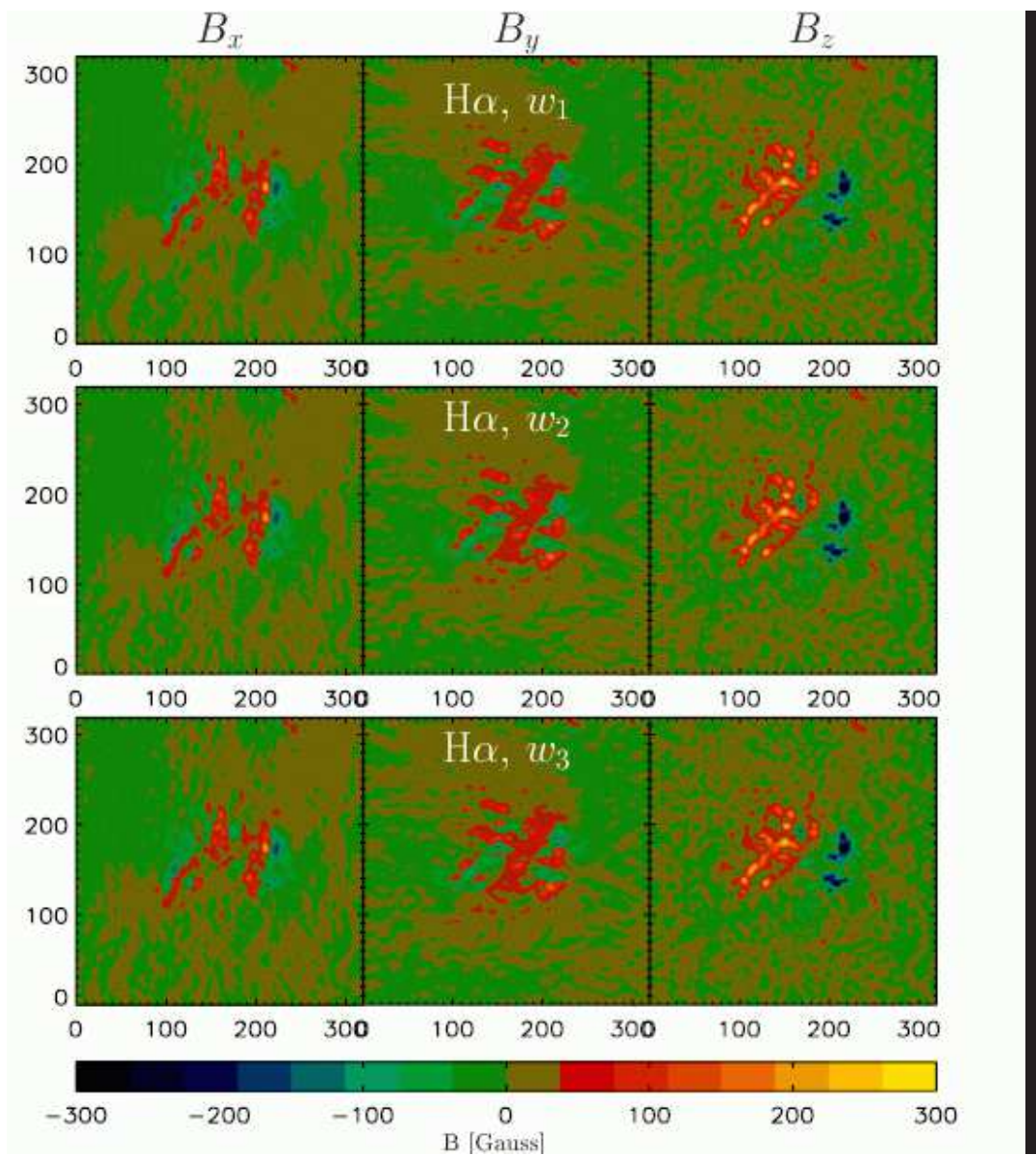


**Figure 5.** Results of  $H\alpha$  preprocessing with different weighting functions. Top:  $w_1$ , Center:  $w_2$ , Bottom:  $w_3$ , see text.

347 inconsistent (forced, noisy) photospheric measurements. The classical preprocessing  
 348 ( $B_{cp}$ ) has already reduced the angle to the model  $H\alpha$  fibrils (last two columns of  
 349 Table 1) by almost a factor of two, even though no information about the chromo-  
 350 sphere has been used. If we include chromospheric information, (see Figure 4) in  
 351 our preprocessing routine ( $B_{H\alpha p}$ , rows 4-7) the angle of the preprocessed field with  
 352 the  $H\alpha$  images reduces significantly. The second to last row in Table 1 contains the

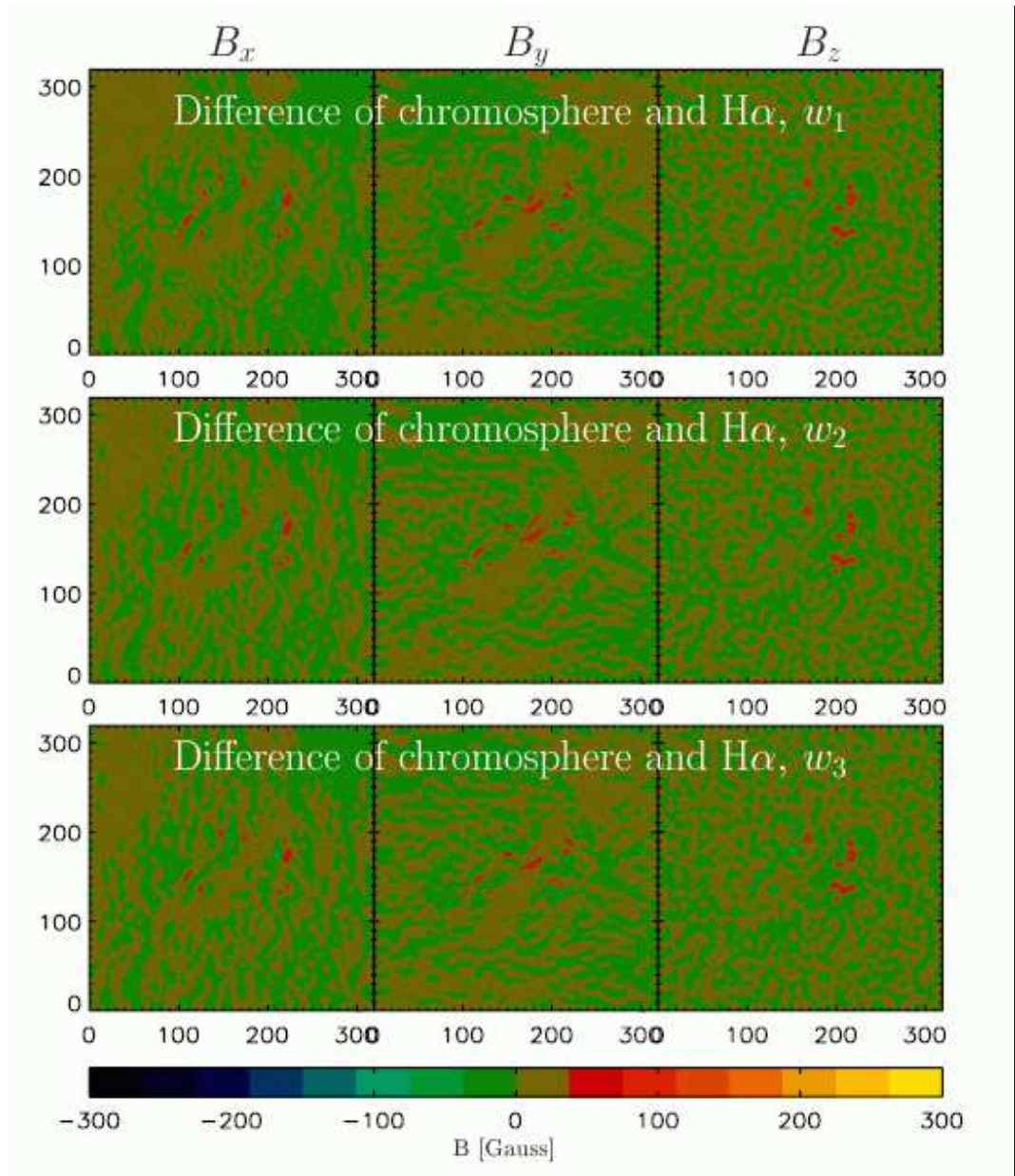


**Figure 6.** Differences of the chromospheric model field (see top panel of Figure 2 and the H $\alpha$ -preprocessed fields as shown in Figure 5.

353 average angle and in the last column the angle has been weighted by the magnetic  
 354 field, which means that  $\phi_{\text{ave},w}$  measures mainly how well the magnetic field and the  
 355 chromospheric fibrils are aligned in regions of a high magnetic field strength. For the  
 356 purpose of coronal magnetic field extrapolations the strong field regions are essential.  
 357 If we include all information from the  $\text{H}\alpha$  image, as done in row 4 for  $w_1$  we find  
 358 that the magnetic field and the fibrils are almost parallel in the entire region. This  
 359 is the ideal case, however, as fibrils have been identified all over the region with the  
 360 same excellent accuracy. For observed data it is more likely that the direction of the  
 361 fibrils will be identifiable with high accuracy only in bright and magnetically strong  
 362 regions. This effect is taken into account in rows 5-7 of both tables. In the last two  
 363 rows we take the chromospheric data only into account where the magnetic field  
 364 strength is larger than 50% and 10% of the maximum field strength, respectively.  
 365 Naturally, the average angle  $\phi_{\text{ave}}$  of the chromospheric fibrils with the preprocessed  
 366 magnetic field becomes larger than for the ideal case. We find, however, that the  
 367 angle  $\phi_{\text{ave},w}$  remains relatively low in strong field regions, except for the case  $w_3$ .

368 We can easily understand that  $w_3$  (chromospheric information ignored where  
 369 the magnetic field is less than 50% of its maximum) provides less accurate results,  
 370 because the area where chromospheric data have been taken into account, is only a  
 371 very small fraction of the entire region (see Figure 4 lower central panel).

372 Case  $w_3$  has few nonzero points. These points are, however, in the regions with  
 373 the strongest magnetic field strength. The  $L_5$  terms minimize the angle between  
 374 magnetic field and chromospheric fibrils only in these nonzero points. This local  
 375 correction does, however, influence the magnetogram globally, because the  $L_1$  and  
 376  $L_2$  term contain global measures and the  $L_4$  terms couple neighbouring points. As  
 377 a consequence the preprocessing result is different from classical preprocessing, even  
 378 if the  $L_5$  term is nonzero only for a limited number of pixel.

379 For observational data the weighting  $w_4$  (last row in the tables, areas with less  
 380 than 10% ignored; see also 4 lower right panel) seems to be more realistic. In this  
 381 case the overall average angle is not better than for classical preprocessing, but is  
 382 different by only about  $3^\circ$  when preferential weighting is given to the more important  
 383 strong field regions.

384 The ultimate test regarding the success of our extended preprocessing scheme is  
 385 to use the preprocessed field as boundary conditions for a nonlinear force-free coronal  
 386 magnetic field extrapolation. The results are presented in Table 2, row 3 for classical  
 387 preprocessing and rows 4-7 for  $\text{H}\alpha$  preprocessing. We find that all preprocessed  
 388 fields provide much better results than using the unprocessed data. For classical  
 389 preprocessing we get the magnetic energy  $\epsilon_{\text{mag}}$  correct with an error of 3% (for  
 390 unprocessed data we got an error of 35%). Taking the  $\text{H}\alpha$  information into account  
 391 improves the result and the magnetic energy is computed with an accuracy of 1% or  
 392 better, even for the cases where we used chromospheric information only in parts of  
 393 the entire regions.

## 394 6. Conclusions and Outlook

395 Within this work we developed an improved algorithm for the preprocessing of  
 396 photospheric vector magnetograms for the purpose of getting suitable boundary  
 397 conditions for nonlinear force-free extrapolations. We extended the preprocessing  
 398 routine developed by Wiegelmann, Inhester, and Sakurai (2006), which is referred to



**Table 1.** Results of the various preprocessing schemes: the model chromosphere and photosphere (first two rows), classical preprocessing (third row), and the H $\alpha$  preprocessing cases (last four rows). Column 1 identifies the data set, columns 2 and 3 the value of  $\mu_5$  and the weighting scheme used for the H $\alpha$  preprocessing cases. Columns 4-7 provide the value of the functionals  $L_{12} = L_1 + L_2$ ,  $L_3$ ,  $L_4$ ,  $L_5$  as defined in Equations (12)-(15) and (17), respectively. In columns 8 and 9 we show how well the force-free and torque-free consistency criteria ( $\varepsilon_{\text{force}}$ ,  $\varepsilon_{\text{torque}}$ ) as defined in Equations (9) and (10) are fulfilled. The last two columns contain the averaged angle ( $\phi_{\text{ave}} = \langle \phi(x, y) \rangle$ ) of the field with the model chromospheric data and a magnetic field weighted average angle ( $\phi_{\text{ave,w}} = \frac{\langle B^2 \phi(x, y) \rangle}{\langle B^2 \rangle}$ ) with  $\phi(x, y)$  as defined in Equation (16).

Data	Weights		$L_{\text{prep}} \times 10^{-6}$				Aly criteria		$\phi_{\text{ave}}$ [deg]	$\phi_{\text{ave,w}}$ [deg]
	$\mu_5$	$w$	$L_{12}$	$L_3$	$L_4$	$L_5$	$\varepsilon_{\text{force}}$	$\varepsilon_{\text{torque}}$		
$B_{\text{ch}}$	-	-	452.137	3.57	0.18	0.00	0.0171	0.0203	-	-
$B_{\text{np}}$	-	-	338287.	0.00	4.45	0.49	0.4138	0.5797	19.2	18.9
$B_{\text{cp}}$	-	-	0.06658	2.30	0.18	0.21	0.0003	0.0001	10.1	8.8
$B_{\text{H}\alpha\text{p}}$	1.525	w <sub>1</sub>	33.37	2.45	0.17	0.0007	0.0062	0.0011	1.1	0.4
$B_{\text{H}\alpha\text{p}}$	1.765	w <sub>2</sub>	31.70	2.47	0.15	0.0171	0.0060	0.0012	7.3	2.0
$B_{\text{H}\alpha\text{p}}$	1.880	w <sub>3</sub>	29.10	2.41	0.15	0.1355	0.0058	0.0012	10.8	6.8
$B_{\text{H}\alpha\text{p}}$	2.115	w <sub>4</sub>	32.16	2.41	0.17	0.0531	0.0060	0.0012	10.4	3.1

**Table 2.** Results of the nonlinear force-free field extrapolations in a 3D box ( $320 \times 320 \times 256$ ). The rows are the same as in Table 1. The first three columns identify the preprocessing scheme, the value of  $\mu_5$ , and the weighting scheme as in Table 1. The fourth column contains the functional  $L$ , as defined in Equation (21), which tells us how well the force-free and solenoidal conditions are fulfilled in the computational box. In columns 5-9 we compare the extrapolated 3D magnetic field with the reference solution and use different quantitative comparison metrics: the vector correlation ( $C_{\text{vec}}$ ), the Cauchy-Schwarz metric ( $C_{\text{cs}}$ ), the complement of the normalized vector error ( $E'_{\text{n}}$ ), the complement of the mean vector error ( $E'_{\text{m}}$ ), and the total magnetic energy normalized to the reference field ( $\epsilon_{\text{mag}}$ ) as defined in Equations (22)-(26), respectively. Perfect agreement for any of these comparison metrics is unity.

Data	$\mu_5$	$w$	$L$	$C_{\text{vec}}$	$C_{\text{cs}}$	$E'_{\text{n}}$	$E'_{\text{m}}$	$\epsilon_{\text{mag}}$
$B_{\text{ch}}$	-	-	0.53	1.00	1.00	1.00	1.00	1.00
$B_{\text{np}}$	-	-	46.03	0.91	0.99	0.69	0.85	0.65
$B_{\text{cp}}$	-	-	5.99	0.97	0.99	0.80	0.85	0.97
$B_{\text{H}\alpha\text{p}}$	1.525	w <sub>1</sub>	3.45	0.97	1.00	0.81	0.85	1.01
$B_{\text{H}\alpha\text{p}}$	1.765	w <sub>2</sub>	2.37	0.97	1.00	0.81	0.86	1.00
$B_{\text{H}\alpha\text{p}}$	1.880	w <sub>3</sub>	2.31	0.97	1.00	0.81	0.85	0.99
$B_{\text{H}\alpha\text{p}}$	2.115	w <sub>4</sub>	3.20	0.97	1.00	0.81	0.85	1.00

399 here as “classical preprocessing”. The main motivation for this work is related to the  
400 fact that active-region coronal magnetic fields are force-free due to the low  $\beta$  coronal  
401 plasma, but the magnetic field vector can be measured with high accuracy only on  
402 the photosphere, where the plasma  $\beta$  is about unity and non-magnetic forces cannot  
403 be ignored. Our original (“classical”) preprocessing removes these non-magnetic  
404 forces and makes the field compatible with the force-free assumption leading to more  
405 chromospheric-like configurations. In this study, we have found that by taking direct  
406 chromospheric observations into account (such as by using fibrils seen in H $\alpha$  images),  
407 the preprocessing is improved beyond the classical scheme. This improved scheme  
408 includes a term which minimizes the angle between the preprocessed magnetic field  
409 and the fibrils. We tested our method with the help of a model active region developed  
410 by van Ballegoijen *et al.* (2007), which includes the forced photospheric and force-  
411 free chromospheric and coronal layers. This model has been used by Metcalf *et al.*  
412 (2007) for an inter-comparison of nonlinear force-free extrapolation codes. The  
413 comparison revealed that the model coronal magnetic field was reconstructed very  
414 well if chromospheric magnetic fields have been used as input, but in contrast the  
415 reconstructed fields compared poorly when unprocessed model-photospheric data  
416 were used. Classical preprocessing significantly improves the result, but the H $\alpha$   
417 preprocessing developed in this paper is even better as the main features of the  
418 model corona are reconstructed with high accuracy. Our extended preprocessing  
419 tool provides a fair estimate of the chromospheric magnetic field, which is used as  
420 boundary condition for computing the nonlinear force-free coronal magnetic field.  
421 In particular, the magnetic energy in the force-free domain above the chromosphere  
422 agrees with the model corona within 1%, even if only strong-field regions of the model  
423 chromosphere, where the fibrils can be identified with highest accuracy, influence the  
424 final solution. From these tests we conclude that our improved preprocessing routine  
425 is a useful tool for providing suitable boundary conditions for the computation of  
426 coronal magnetic fields from measured photospheric vector magnetograms as pro-  
427 vided for example from *Hinode*. The combination of preprocessing and nonlinear  
428 force-free field extrapolations seem likely to provide accurate computation of the  
429 magnetic field in the corona.

430 We will still not get the magnetic field structure in the relative thin layer be-  
431 tween/in the photosphere and the chromosphere correct, because here non-magnetic  
432 forces cannot be neglected due to the finite  $\beta$  plasma. Although this layer is vertically  
433 thin (*e.g.*, 2 vertical grid points in the van Ballegoijen *et al.* (2007) model compared  
434 to 256 vertical grid points in the corona) it contains a significant part of the total  
435 magnetic energy of the entire domain, see Metcalf *et al.* (2007). Unfortunately, this  
436 part of the energy cannot be recovered by force-free extrapolations, because the  
437 region is non-force-free. Our improved preprocessing routine includes chromospheric  
438 information and therefore provides us with a closer approximation of the chromo-  
439 spheric magnetic field. This leads to more accurate estimates of the total magnetic  
440 energy in the corona.

441 A further improvement of the preprocessing routine could be done with the help  
442 of additional observations, *e.g.* the line-of-sight chromospheric field, as planned for  
443 SOLIS. One could include these measurement directly in the  $L_3$ -term (14) either as  
444 the only information or in some weighted combination with the photospheric field  
445 measurement. An investigation of the true 3D-structure of the thin non-force-free  
446 layer between photosphere and chromosphere requires further research. First steps  
447 towards non-force-free magnetohydrostatic extrapolation codes (Wiegelmann and

448 Neukirch, 2006) might help to reveal the secrets of this layer. Non force-free magnetic  
449 field extrapolations will require additional observational constraints, because the  
450 magnetic field, the plasma density and pressure must be computed self-consistently  
451 in one model.

452 **Acknowledgements** The work of T. Wiegmann was supported by DLR-grant 50 OC  
453 0501 and J.K. Thalmann got financial support by DFG-grant WI 3211/1-1. M. DeRosa, T.  
454 Metcalf, and C. Schrijver were supported by Lockheed Martin Independent Research funds. We  
455 acknowledge stimulating discussions during the fourth NLFFF-consortium meeting in June,  
456 2007 in Paris.

## 457 Appendix

### 458 A. Extrapolation of Nonlinear Force-free Coronal Magnetic Fields

459 We briefly summarize our nonlinear force-free extrapolation code here, which has  
460 been used to compute the 3D magnetic fields. We solve the force-free Equations (1)  
461 and (2) by optimizing (minimizing) the following functional:

$$L = \int_V \left[ w_a B^{-2} |(\nabla \times \mathbf{B}) \times \mathbf{B}|^2 + w_b |\nabla \cdot \mathbf{B}|^2 \right] d^3x, \quad (21)$$

462 where  $w_a(x, y, z)$  and  $w_b(x, y, z)$  are weighting functions. It is obvious that (for  
463  $w_a, w_b > 0$ ) the force-free equations (1) and (2) are fulfilled when  $L$  is zero. The  
464 optimization method was proposed by Wheatland, Sturrock, and Roumeliotis (2000)  
465 and further developed in Wiegmann and Neukirch (2003). Here we use the imple-  
466 mentation of Wiegmann (2004) which has been applied to data in Wiegmann et  
467 al. (2005). In this article, we used a recent update including of our code that included  
468 a multi-scale approach (see Metcalf et al. (2007) for details). This version of the op-  
469 timization code was also used with the (same as in this paper) model-chromospheric,  
470 photospheric and classical preprocessed photospheric magnetic field vector as part of  
471 an inter-code-comparison in (Metcalf *et al.*, 2007). For alternative methods to solve  
472 the force-free Equations (1) and (2) see the review papers by (Sakurai, 1989; Aly,  
473 1989; Amari *et al.*, 1997; McClymont, Jiao, and Mikic, 1997; Wiegmann, 2008) and  
474 references therein.

### 475 B. Metrics to Compare a 3D Coronal Magnetic Field with a Reference 476 Solution.

477 In order to quantify the degree of agreement between the extrapolated vector fields of  
478 the input model field ( $\mathbf{B}$ , *i.e.*, the extrapolated chromospheric (reference) field) and  
479 the nonlinear force-free solutions ( $\mathbf{b}$ , *i.e.*, the extrapolated preprocessed photospheric  
480 field) that are specified on identical sets of grid points, we use five metrics in table 2  
481 that compare either local characteristics or the global energy content in addition to  
482 the force and divergence integrals. These measures have been developed in Schrijver  
483 et al. (2006) and subsequently been used to evaluate the quality of force-free and non-  
484 force-free extrapolation codes (Amari, Boulmezaoud, and Aly, 2006; Wiegmann

485 *et al.*, 2006; Wiegelmann and Neukirch, 2006; Song *et al.*, 2006; Wiegelmann, 2007;  
486 Metcalf *et al.*, 2007).

487 The vector correlation metric has been defined as

$$C_{\text{vec}} = \frac{\sum_i \mathbf{B}_i \mathbf{b}_i}{\sqrt{\sum_i |\mathbf{B}_i|^2 \sum_i |\mathbf{b}_i|^2}}, \quad (22)$$

488 where  $\mathbf{B}_i$  and  $\mathbf{b}_i$  are the vectors at each point  $i$ . One finds that  $C_{\text{vec}} = 1$  if the  
489 vector fields are identical and  $C_{\text{vec}} = 0$  if  $\mathbf{B}_i \perp \mathbf{b}_i$ .

490 The Cauchy-Schwarz metric is based on the homonymous inequality ( $|\mathbf{a} \cdot \mathbf{c}| \leq |\mathbf{a}| |\mathbf{c}|$ )  
491 for any two vectors  $\mathbf{a}$  and  $\mathbf{c}$ )

$$C_{\text{cs}} = \frac{1}{M} \sum_i \frac{\mathbf{B}_i \cdot \mathbf{b}_i}{|\mathbf{B}_i| |\mathbf{b}_i|} \equiv \frac{1}{M} \sum_i \cos \theta_i, \quad (23)$$

492 where  $M$  is the total number of vectors in the volume, and  $\theta_i$  the angle between  $\mathbf{B}$   
493 and  $\mathbf{b}$  at point  $i$ . It is entirely a measure of the angular differences of the vector  
494 fields, i. e.  $C_{\text{cs}} = 1$  if  $\mathbf{B} \parallel \mathbf{b}$ ,  $C_{\text{vec}} = -1$  if they are anti-parallel, and  $C_{\text{vec}} = 0$  if  
495  $\mathbf{B}_i \perp \mathbf{b}_i$  at each point.

496 The normalized vector error is defined as

$$E_{\text{n}} = \frac{\sum_i |\mathbf{b}_i - \mathbf{B}_i|}{\sum_i |\mathbf{B}_i|}. \quad (24)$$

497 The mean vector error averages over relative differences and is given by

$$E_{\text{m}} = \frac{1}{M} \sum_i \frac{|\mathbf{b}_i - \mathbf{B}_i|}{|\mathbf{B}_i|}. \quad (25)$$

498 Unlike the first two metrics, perfect agreement of the two vector fields results in  
499  $E_{\text{m}} = E_{\text{n}} = 0$ . For an easier comparison with the others, we list  $E'_{\text{m,n}} \equiv 1 - E_{\text{m,n}}$ ,  
500 so that all measures reach unity for a perfect match.

501 To estimate how well the models rates the energy content of the field, we use the  
502 total magnetic energy of  $\mathbf{b}$ , normalized to the total magnetic energy of  $\mathbf{B}$ , namely

$$\epsilon_{\text{mag}} = \frac{\sum_i |\mathbf{b}_i|^2}{\sum_i |\mathbf{B}_i|^2}. \quad (26)$$

## 503 References

- 504 Aly, J.J.: 1989, On the reconstruction of the nonlinear force-free coronal magnetic field from  
505 boundary data. *Sol. Phys.* **120**, 19–48.  
506 Amari, T., Aly, J.J., Luciani, J.F., Boulmezaoud, T.Z., Mikic, Z.: 1997, Reconstructing the  
507 Solar Coronal Magnetic Field as a Force-Free Magnetic Field. *Sol. Phys.* **174**, 129–149.  
508 Amari, T., Boulmezaoud, T.Z., Aly, J.J.: 2006, Well posed reconstruction of the solar coronal  
509 magnetic field. *A&A* **446**, 691–705. doi:10.1051/0004-6361:20054076.  
510 Gary, G.A.: 2001, Plasma Beta above a Solar Active Region: Rethinking the Paradigm. *Sol.*  
511 *Phys.* **203**, 71–86.

- 512 Inhester, B., Feng, L., Wiegelmann, T.: 2007, Segmentation of loops from coronal EUV images.  
513 *Sol. Phys.* **in press**.
- 514 Kramar, M., Inhester, B., Solanki, S.K.: 2006, Vector tomography for the coronal magnetic  
515 field. I. Longitudinal Zeeman effect measurements. *A&A* **456**, 665–673. doi:10.1051/0004-  
516 6361:20064865.
- 517 Lin, H., Kuhn, J.R., Coulter, R.: 2004, Coronal Magnetic Field Measurements. *ApJL* **613**,  
518 L177–L180. doi:10.1086/425217.
- 519 Low, B.C., Lou, Y.Q.: 1990, Modeling solar force-free magnetic fields. *ApJ* **352**, 343–352.
- 520 McClymont, A.N., Jiao, L., Mikic, Z.: 1997, Problems and Progress in Computing Three-  
521 Dimensional Coronal Active Region Magnetic Fields from Boundary Data. *Sol. Phys.* **174**,  
522 191–218.
- 523 Metcalf, T.R., DeRosa, M.L., Schrijver, C.J., Barnes, G., VanBallegooijen, A., Wiegelmann, T.,  
524 Wheatland, M.S., Valori, G., McTiernan, J.M.: 2007, Non-linear force-free modeling of  
525 coronal magnetic fields. II. Modeling a filament arcade from simulated chromospheric and  
526 photospheric vector fields. *Sol. Phys.* **accepted**.
- 527 Metcalf, T.R., Jiao, L., McClymont, A.N., Canfield, R.C., Uitenbroek, H.: 1995, Is the solar  
528 chromospheric magnetic field force-free? *ApJ* **439**, 474–481. doi:10.1086/175188.
- 529 Molodensky, M.M.: 1969, Integral properties of force-free fields. *Soviet Astron.-AJ* **12**, 585–  
530 588.
- 531 Molodensky, M.M.: 1974, Equilibrium and stability of force-free magnetic field. *Sol. Phys.* **39**,  
532 393–404.
- 533 Sakurai, T.: 1981, Calculation of Force-Free Magnetic Field with Non Constant Alpha. *Sol.*  
534 *Phys.* **69**, 343–+.
- 535 Sakurai, T.: 1989, Computational modeling of magnetic fields in solar active regions. *Space*  
536 *Science Reviews* **51**, 11–48.
- 537 Schrijver, C.J., DeRosa, M.L., Metcalf, T.R., Liu, Y., McTiernan, J., Régnier, S., Valori, G.,  
538 Wheatland, M.S., Wiegelmann, T.: 2006, Nonlinear Force-Free Modeling of Coronal Mag-  
539 netic Fields Part I: A Quantitative Comparison of Methods. *Sol. Phys.* **235**, 161–190.  
540 doi:10.1007/s11207-006-0068-7.
- 541 Schrijver, C.J., van Ballegooijen, A.A.: 2005, Is the Quiet-Sun Corona a Quasi-steady, Force-  
542 free Environment? *ApJ* **630**, 552–560. doi:10.1086/431754.
- 543 Solanki, S.K., Lagg, A., Woch, J., Krupp, N., Collados, M.: 2003, Three-dimensional magnetic  
544 field topology in a region of solar coronal heating. *Nature* **425**, 692–695.
- 545 Song, M.T., Fang, C., Tang, Y.H., Wu, S.T., Zhang, Y.A.: 2006, A New and Fast Way to  
546 Reconstruct a Nonlinear Force-free Field in the Solar Corona. *Astrophys. J.* **649**, 1084–  
547 1092. doi:10.1086/506249.
- 548 van Ballegooijen, A.A.: 2004, Observations and Modeling of a Filament on the Sun. *ApJ* **612**,  
549 519–529. doi:10.1086/422512.
- 550 van Ballegooijen, A.A., Deluca, E.E., Squires, K., Mackay, D.H.: 2007, Modeling magnetic flux  
551 ropes in the solar atmosphere. *Journal of Atmospheric and Terrestrial Physics* **69**, 24–31.  
552 doi:10.1016/j.jastp.2006.06.007.
- 553 Wheatland, M.S., Sturrock, P.A., Roumeliotis, G.: 2000, An Optimization Approach to  
554 Reconstructing Force-free Fields. *ApJ* **540**, 1150–1155.
- 555 Wiegelmann, T.: 2004, Optimization code with weighting function for the reconstruction of  
556 coronal magnetic fields. *Sol. Phys.* **219**, 87–108.
- 557 Wiegelmann, T.: 2007, Computing Nonlinear Force-Free Coronal Magnetic Fields in Spherical  
558 Geometry. *Sol. Phys.* **240**, 227–239. doi:10.1007/s11207-006-0266-3.
- 559 Wiegelmann, T.: 2008, Nonlinear force-free modeling of the solar coronal magnetic field.. *J.*  
560 *Geophys. Res.* **VOL. 113**, A03S02, doi:10.1029/2007JA012432.
- 561 Wiegelmann, T., Inhester, B., Kliem, B., Valori, G., Neukirch, T.: 2006, Testing non-linear  
562 force-free coronal magnetic field extrapolations with the Titov-Démoulin equilibrium. *A&A*  
563 **453**, 737–741. doi:10.1051/0004-6361:20054751.
- 564 Wiegelmann, T., Inhester, B., Lagg, A., Solanki, S.K.: 2005, How To Use Magnetic Field  
565 Information For Coronal Loop Identification. *Sol. Phys.* **228**, 67–78. doi:10.1007/s11207-  
566 005-2511-6.
- 567 Wiegelmann, T., Inhester, B., Sakurai, T.: 2006, Preprocessing of vector magnetograph data  
568 for a nonlinear force-free magnetic field reconstruction. *Sol. Phys.* **233**, 215–232.
- 569 Wiegelmann, T., Neukirch, T.: 2003, Computing nonlinear force free coronal magnetic fields.  
570 *Nonlinear Processes in Geophysics* **10**, 313–322.
- 571 Wiegelmann, T., Neukirch, T.: 2006, An optimization principle for the computation of MHD  
572 equilibria in the solar corona. *A&A* **457**, 1053–1058. doi:10.1051/0004-6361:20065281.

